

In situ semi-quantitative analysis of zinc dissolution within nanoporous silicon by X-ray absorption fine-structure spectroscopy employing an X-ray compatible cell

Álvaro Muñoz-Noval,^{a,*} ‡ Kazuhiro Fukami,^b Akira Koyama,^{b,c} Takuya Kuruma^a and Shinjiro Hayakawa^a

Received 19 June 2018

Accepted 19 October 2018

Edited by M. Yamamoto, RIKEN SPring-8 Center, Japan

‡ Current address: Department of Physics of Materials, Universidad Complutense de Madrid, 28080 Madrid, Spain.

Keywords: zinc negative electrodes; *in situ* XAFS cell; porous electrodes.

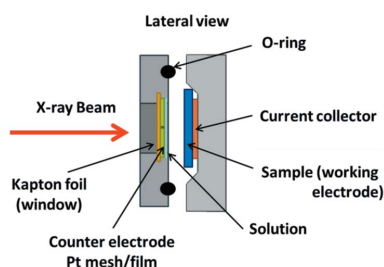
Supporting information: this article has supporting information at journals.iucr.org/s

^aDepartment of Applied Chemistry, Graduate School of Engineering, Hiroshima University, Hiroshima 739-8527, Japan, ^bDepartment of Materials Science and Engineering, Graduate School of Engineering, Kyoto University, Kyoto 606-8501, Japan, and ^cDivision of Applied Chemistry, Graduate School of Engineering, Hokkaido University, Sapporo 060-8628, Japan. *Correspondence e-mail: almuno06@ucm.es

The *in situ* study of the discharge process in a zinc-based half-cell employing a porous electrode as a structural scaffold is reported. The *in situ* characterization has been performed by synchrotron X-ray absorption fine-structure spectroscopy and, for this purpose, an inexpensive, simple and versatile electrochemical cell compatible with X-ray experiments has been designed and described. The experimental results reported here have been employed to semi-quantify the dissolved and undissolved zinc species during the discharge, allowing the cell feasibility to be tested and to better understand the functioning of the zinc half-cell based on porous electrodes.

1. Introduction

Metallic zinc has been considered a promising material to be employed as the negative electrode for next-generation batteries. The utilization of zinc and other elemental materials as negative electrodes increases the achievable energy density in batteries with respect to lithium ion batteries (Kim *et al.*, 2013; Li & Dai, 2014; Xu *et al.*, 2014; Li *et al.*, 2014). However, during the charge of a metallic zinc negative electrode, dendritic growth of zinc is often observed, being enhanced for high charging currents (Koda *et al.*, 2013). This aspect represents a crucial drawback for the applicability of zinc-based negative electrodes. The authors have been proposing to utilize a nanoporous electrode for the host matrix of zinc deposits as a strategy to avoid dendritic growth, since the shape of the deposit is strictly controlled by the morphology of nanopores. In general, conducting or semiconducting porous electrodes have a slow diffusion in the pore and, therefore, electrochemical reactions preferentially proceed on the more surficial region of the porous layer, namely on the pore wall near the pore opening. We have studied how to enhance the mass-transport within nanopores, and have found that the enhancement of hydrophobic effects between metal precursors and pore surface is key to accelerate electrodeposition within the porous structure of a nanoporous electrode (Kinoshita, 2000, 2004). In the particular case of zinc electrodeposition, under appropriate conditions (Koyama *et al.*, 2016; Muñoz-Noval *et al.*, 2017) the zinc cation–polycarboxylate complex was greatly enriched within the nanopores and the subsequent zinc electrodeposition highly accelerated. As a result, we succeeded in the suppression of



zinc dendritic growth under a high current density. This mechanism was recently evaluated by the analysis of X-ray absorption fine-structure spectroscopy (XAFS), showing the power of this tool to provide a molecular-scale picture of the accelerated electrodeposition within nanopores.

In the present study, we have designed a compatible cell for an X-ray beamline to be used for *in situ* measurements. This paper describes the *in situ* study of discharge processes of metallic zinc within porous electrodes fabricated with porous silicon. This work is a step forward in the evaluation and development of zinc negative electrodes.

2. Experimental

2.1. Substrate and electrolyte

Microporous silicon electrodes (PSi) with pore diameter of 3 nm and porous layer thickness of 2 μm were prepared starting from an n-Si (100) with a resistivity of 10–20 Ω cm as a substrate. Anodization of the silicon wafer in 22 wt% HF electrolyte solution (48 wt% HF:ethanol = 1:1.7 in volume) was carried out with a current density of 2.0 mA cm⁻² and the duration of anodization was ~20 min. Note that illumination of substrates is necessary for anodization of n-type semiconductors. This anodization of Si results in a PSi electrode with ~60% porosity, which was measured by dividing the weight difference before and after the anodization by that before the anodization and after the removal of the porous layer.

Electrodeposition of zinc was performed under a current density of -10 mA cm⁻² using different zinc complexes, starting with 0.1 M ZnSO₄ and adding 0.1 M disodium malonate (adjusting the pH to 2.0, 3.0, 4.0, 5.0 with a small amount of H₂SO₄) or 0.3 M disodium citrate (adjusting the pH in the same way). Durations of electrodeposition were selected to be between 20 and 120 s. After the electrochemical filling of pores with metallic Zn, the filling ratio reaches ~75%. Until this step, the electrochemical treatments were conducted in a home-made Teflon (beaker-type) cell. For details, the porous silicon electrode was first prepared using a beaker-type cell [with a large amount of electrolyte solution (~20 ml)]. Immediately after the preparation of the porous silicon electrode, zinc was electrochemically deposited within the nanopores of porous silicon. This deposition corresponds to the initial charging. The initial charging was also performed using the beaker-type cell with ~20 ml of Zn-malonate solution. After the preparation of the Zn-embedded porous silicon electrode, the electrochemical cell shown in Fig. 1(a) was constructed.

nate (adjusting the pH to 2.0, 3.0, 4.0, 5.0 with a small amount of H₂SO₄) or 0.3 M disodium citrate (adjusting the pH in the same way). Durations of electrodeposition were selected to be between 20 and 120 s. After the electrochemical filling of pores with metallic Zn, the filling ratio reaches ~75%. Until this step, the electrochemical treatments were conducted in a home-made Teflon (beaker-type) cell. For details, the porous silicon electrode was first prepared using a beaker-type cell [with a large amount of electrolyte solution (~20 ml)]. Immediately after the preparation of the porous silicon electrode, zinc was electrochemically deposited within the nanopores of porous silicon. This deposition corresponds to the initial charging. The initial charging was also performed using the beaker-type cell with ~20 ml of Zn-malonate solution. After the preparation of the Zn-embedded porous silicon electrode, the electrochemical cell shown in Fig. 1(a) was constructed.

2.2. XAFS experiments at BL01 at SPring-8

The XAFS data acquired at the Zn K-edge (9600 eV) in fluorescence yield mode were obtained at BL01 at SPring-8 (Hyogo, Japan). A single spectrum for each stage of the electrochemical process was enough to obtain spectra with sufficient quality. For testing the sample homogeneity in non-time-dependent measurements, several scans were obtained at each sample. Spectra were acquired upon wavenumber values of 15 Å⁻¹.

The dynamic measurements between cycles were performed under charging and discharging of the working electrode. The acquisition time of a complete scan took ~8 min, which was long enough to ensure that the conditions

were kept stable during the measurement. The spectral measurements were performed *in situ* under the electrochemical dissolution of metallic zinc deposited within the porous silicon electrode at a constant current density of +19 μA cm⁻². For calculating the Fourier transform (FT) of the EXAFS signal, a *k*-window from 2.5 to 11 Å⁻¹ was selected for all the spectra. Standard procedures were applied for reducing EXAFS data by using the *Demeter* package (Ravel & Newville, 2005).

2.3. Cell design and experimental procedure

The XAFS-compatible electrochemical cell was a home-made design based on a standard cell that we have employed for PSi etching and electrodeposition. The general scheme of the cell is shown in Fig. 1. The X-ray window in the front part has a truncated cone shape. This window was made of

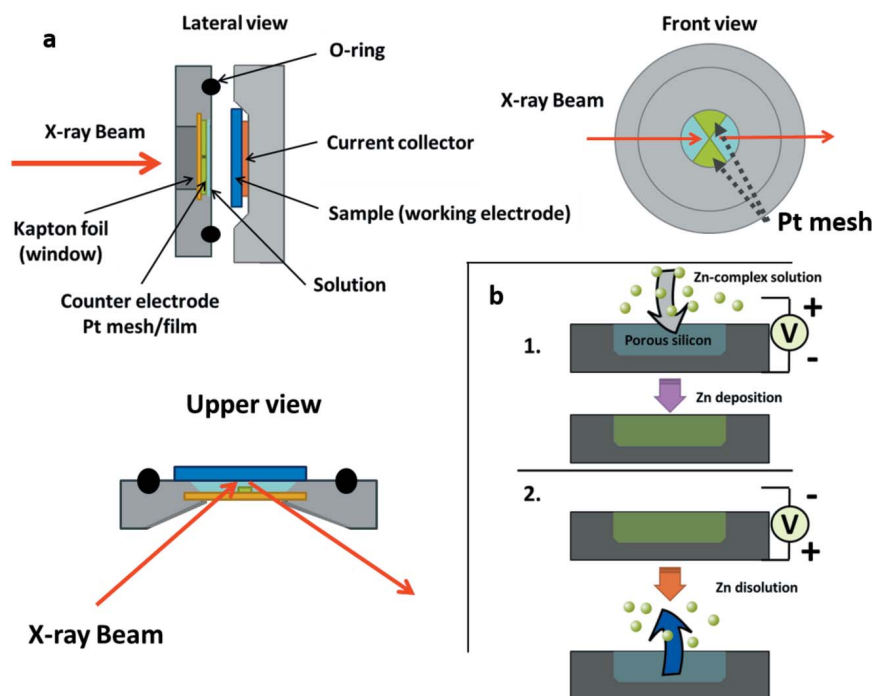


Figure 1
(a) Schematics of the electrochemical cell for XAFS, showing the different parts. (b) Schematics of the process of charge (Zn deposition) and discharge (Zn dissolution) of the Zn-PSi half-cell.

kapton foil, and was attached to keep the electrochemical bath confined in the electrolyte recipient (separator). A porous glass microfiber filter (Whatman, GF/A) was used as separator. The diameter of the separator was large enough to cover the porosified region on the silicon wafer. A total of $\sim 100 \mu\text{L}$ electrolyte solution was placed in the separator space. During the Zn discharge process in the half-cell, Zn tends to be deposited at the counter-electrode which is usually placed to face the porous surface of the working electrode. Because the Zn deposit on the counter-electrode masks the Zn signal from the cell (solution and substrate), we fabricated a butterfly-shaped Pt counter-electrode which maximized the surface of the electrode and, at the same time, allows the X-ray beam to pass through without interaction with the electrode-deposited Zn in the electrode. In the current experiment a Pt mesh electrode is employed, but we also noticed that evaporating Pt in the kapton foil of the window, employing a mask to shape it, was also feasible for this purpose.

During a charge process, Zn is deposited in nanopores of PSi from a Zn-malonate bath. Details of this process, the suitability of employing this electrochemical bath and its chemical recipes have already been discussed (Koyama *et al.*, 2016; Muñoz-Noval *et al.*, 2017). The discharge of the half-cell consists of the opposite process, *i.e.* the metallic Zn nano-

particles within the nanopores are oxidized and dissolved, followed by the formation of the Zn complex with malonate in the solution.

3. Results

The discharging (Zn dissolution) process of the half-cell has been followed *in situ* by recording the XAFS signal. In Fig. 2, we show the XAFS spectra (including XANES and EXAFS) of the half-cell discharging at a constant voltage (1 V). Briefly, as the Zn dissolution takes place, the XANES spectrum shows a larger contribution from Zn in the electrolyte, illustrated in Fig. 2(a). The height of the white line is related to the aqueous phase of Zn (both malonate and anionic) and therefore is proportional to the fraction of dissolved Zn. Actually, it is possible to observe this effect in Fig. 2(b). In parallel, the contribution of the Zn metallic phase vanishes caused by the Zn dissolution. The main observable feature is the pre-peak shoulder from the metal phase, which decreases in intensity along the dissolution [Fig. 2(c)].

The whole process was also registered by the EXAFS signal (Fig. 3). The FT of the combined EXAFS signal from the electrolyte and Zn nano-deposits in the porous substrate shows a convoluted double peak, due to the Zn–O shell in the aqueous Zn-malonate and the Zn-malonate at the solution/PSi interface. A third peak of lower intensity is observed at the corresponding position to the Zn–Zn first shell of metallic Zn. The relative intensity of the first peak (Zn–O from aqueous state) with respect to the other two (Zn–O from the Zn-malonate at the interface and Zn–Zn from the Zn deposits) increases progressively as the Zn dissolution proceeds.

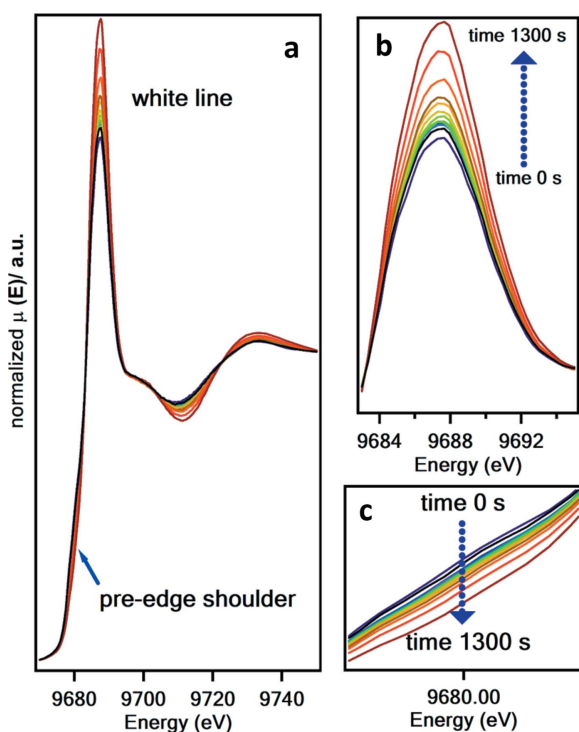


Figure 2 XANES spectra acquired at different stages of the discharge during the *in situ* XAFS experiment on Zn-embedded porous silicon. Metallic zinc was deposited in advance within the porous silicon electrode at a capacity of $\sim 1.2 \text{ C cm}^{-2}$. (a) Complete XANES spectra of the cell during the dissolution of the zinc; (b) detail of the white line showing the increase of the intensity of the main peak as a consequence of the increase of the dissolved Zn-complex phase during the discharge; (c) detail of the pre-peak shoulder showing the vanishing of the shoulder of the metallic phase as a consequence of the dissolution; in (b) and (c) the arrows show the evolution of the spectra during the discharge (dissolution).

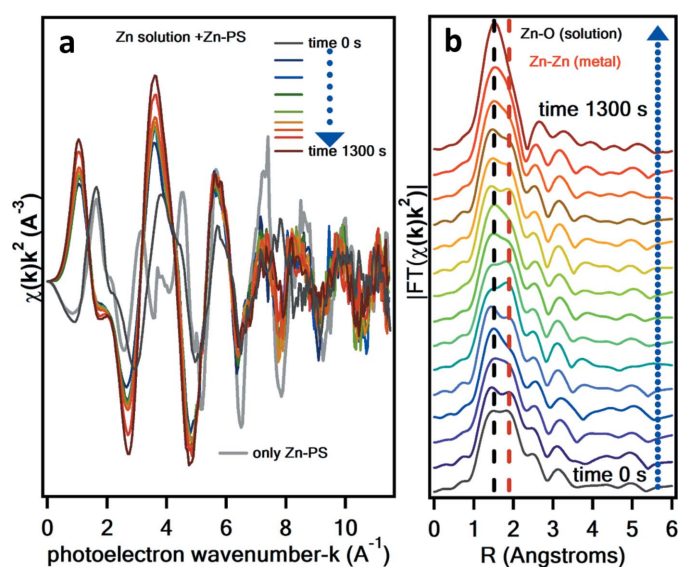
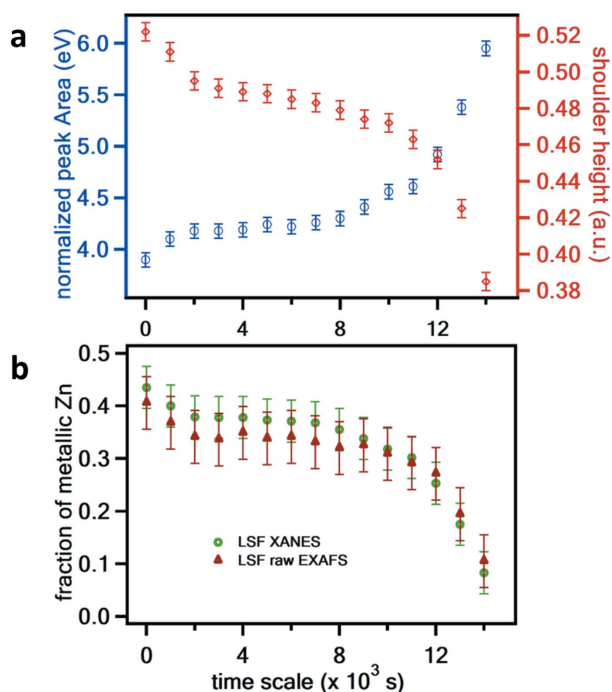


Figure 3 EXAFS spectra acquired during the discharging process of the zinc half-electrode. (a) EXAFS signal as function of the photoelectron wavevector taken at different times during the zinc dissolution in the porous electrode; (b) corresponding Fourier transform of the EXAFS presented in (a) showing the main contribution of the Zn–O and Zn–Zn shells to the spectra. The arrow shows the direction of the process during the dissolution.


Figure 4

Discharge process (Zn dissolution from the porous half-cell) followed by the XAFS spectral features (a) shoulder height (metallic phase) and main peak area (Zn-chelate aqueous phase); and (b) Zn fraction in the cell semi-quantified by least-squares linear combination fitting of the XANES spectra using metallic Zn and Zn-malonate solution references.

The evolution of the phase contribution along the discharge has been monitored quantifying the main spectral features of the XANES spectra. In Fig. 4(a) the main peak area and the pre-edge shoulder height as a function of the dissolution time are depicted. Both parameters (proportional to the relative concentration of each phase) show an opposite but correlated behavior during the dissolution of metallic zinc deposits.

Alternatively, to semi-quantify the Zn speciation in the electrochemical cell during the process, the XANES spectra have been fitted by least-square linear combination by employing pure metallic Zn and Zn-malonate liquid spectra as references. As shown by the fitting presented in Fig. 4(b), the fraction of metallic Zn in the optical path is below 50% in mass, even before the dissolution starts. In the time-dependent dissolution curves [Figs. 4(a) and 4(b)], three clear regimes can be observed. The dissolution at the first stage shows an abrupt decrease of metallic Zn content in the cell, and thus one could say it is linear within the experimental resolution. The second stage, which corresponds to the major part of the discharging cycle, shows a smooth and linear decrease of zinc in the cell and therefore the constant current is consumed mostly for the dissolution of metallic zinc. The third and last stage shows a clear change in the dissolution behavior and the dissolution is abruptly accelerated.

4. Discussion

After the qualitative identification of the dissolution of zinc during the discharge, we attempted to semi-quantify both

coexisting chemical species in the electrolyte and in the deposit within the porous electrode based on the raw XAFS data. To simplify, we have assumed that the normalized fluorescence signal (I_F) is basically proportional to the absorbance in this range of concentrations and therefore we have discarded matrix effects,

$$I_F = \alpha \mu_\rho \rho L, \quad (1)$$

where α is a proportionality phenomenological constant, μ_ρ is the absorbance coefficient, ρ is the density and L is the length of the optical path through the material. With this approximation, we estimate the dependency of the fluorescence signal with the physical parameters of the liquid and solid phases in the cell to be

$$I_F^l = \alpha \mu_\rho m_M [\text{Zn}] l, \quad (2)$$

$$I_F^s = \alpha \mu_\rho \rho, \quad (3)$$

for the liquid [equation (2)] and the solid [equation (3)]. Here, m_M is the molar mass of Zn, l is the optical path of the electrolyte in the cell and ρ is the density of Zn in the cell. When the Zn substrate is immersed in the water inside the cell, I_F^s needs to include an attenuation factor due to the aqueous medium in the form $\exp(-\mu_w l)$. Therefore, the fluorescence signal of the whole cell is approximately expressed once the Zn solution is put in place,

$$I_F^l = \alpha \mu_\rho \{m_M [\text{Zn}] l + \rho \exp(-\mu_w l) \exp(-\mu_d l)\}, \quad (4)$$

where a new term $\exp(-\mu_d l)$ has been included, accounting for the attenuation of the signal by the dissolved Zn in the cell. In the experiments, the fluorescence signals of the pre-dissolved samples were measured within the cell before adding any solution, with deionized water and with the electrolyte before starting the dissolution. This allows the attenuation factor of water to be obtained and, hence, not only a qualitative analysis of the dissolution but also a semi-quantification of the Zn in the form of metallic deposits or in the electrolyte to be performed. When the initial values of the signal before and after the addition of water are measured, and when the initial electrolyte is finally placed, we can obtain the initial value of the Zn density in the electrode (ρ), by assuming the initial value of the electrolyte concentration and the optical path length. In our case the initial value is close to 1.27 g cm⁻³ just before the reaction. The value of the Zn density in the porous electrode and Zn concentration in the electrolyte can be estimated along the reaction, considering the values obtained for the main peak height and the shoulder height in the raw XAFS spectra. The shoulder height (related to the amount of metallic Zn) can be mathematically expressed as

$$\text{shoulder height} = \beta \rho \exp([\text{Zn}]), \quad (5)$$

where β is a proportionality constant and the attenuation due to the Zn concentration in the solution has been included. Similarly, the main peak height depends on both the Zn concentration and the metallic Zn density in the porous electrode,

$$\text{main peak height} = \varepsilon[\text{Zn}] + \delta\rho \exp(-[\text{Zn}]). \quad (6)$$

The parameter δ can be obtained from the relation between the main peak height and shoulder height for a spectrum without electrolyte phase ($[\text{Zn}] = 0$). From the experimental parameters before the reaction starts the complete set of experimental parameters can be obtained and hence the time evolution of $[\text{Zn}]$ and ρ {i.e. of $[\text{Zn}](t)$ and $\rho(t)$ }.

The amount of released-Zn/remaining-Zn in the porous electrode during the dissolution process in the zinc anode is estimated from the XAFS signal of the cell. The initial density of Zn can be deduced from the intensity of the fluorescence of the Zn $K\alpha$ signal of the cell without electrolyte or water I_{F0} , the signal with water in the cell I_{Fw} and the signal with the initial electrolyte just before initializing the discharge (assuming a Zn concentration of 0.1 M) I_{FT} . In Fig. 5 we have represented the time dependency of the Zn speciation in the cell along the reaction in the case of the discharging process considering two zinc species. The concentration of Zn in the solution is represented in units of molarity and the density of Zn deposited in the porous electrode is described in units of g cm^{-3} . From the electrochemical conditions, a rough quantitative estimation of the change of Zn deposited in PSi and dissolved in the electrolyte can be performed. Since the discharge proceeded under a constant current density of $+19 \mu\text{A cm}^{-2}$ for $14 \times 10^3 \text{ s}$, the electric charge passed was 0.26 C cm^{-2} . Since the electrode area was 0.785 cm^2 , the metallic Zn dissolved was $2.2 \times 10^{-6} \text{ mol}$ into the solution of $100 \mu\text{L}$. Thus, after a $14 \times 10^3 \text{ s}$ discharge, the electrochemically expected change in concentration of Zn^{2+} is 0.011 M which is several times smaller than that evaluated from XAFS results. A similar discrepancy was obtained in the weight of metallic Zn in PSi (the electrochemical estimation is several times higher than that obtained from the XAFS data). These discrepancies are attributed to the experimental uncertainly summed up to small inaccuracies in the least-squares fitting procedure of the spectra. Although there are

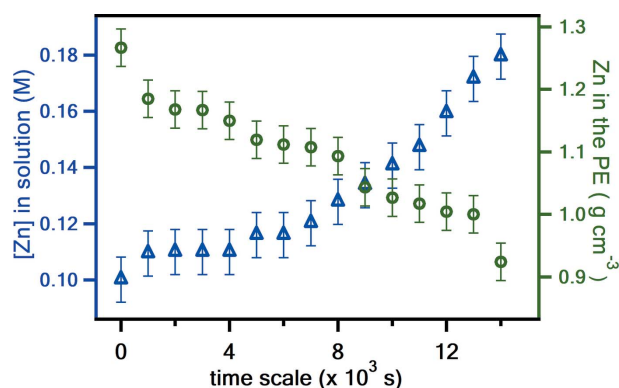


Figure 5 Time-dependent zinc speciation curves for the discharging of the porous electrode with zinc nanoparticles, showing the evolution of the two co-existing zinc species: (circles) metallic zinc deposited within the porous electrode (PE) in the form of nanoparticles and (triangles) zinc malonate dissolved in the electrolyte.

still some quantitative deviations in our analysis, the present study has shown that the contributions of XAFS signals from both the solution and solid are successfully distinguished. However, future experiments will aim for an increase of the quantitative accuracy and refine the spectra fitting procedure, searching for more robust spectral parameters.

5. Conclusions

This work describes the *in situ* characterization, by X-ray absorption fine-structure spectroscopy, of a zinc half-cell in a porous electrode during discharge. An inexpensive, simple and versatile electrochemical cell compatible with X-ray-based experiments has been designed and described throughout the manuscript. Based on the characteristics of the electrochemical system, the results herein presented have been employed to semi-quantify the dissolved and undissolved zinc during the discharge. These experiments have allowed the cell to be tested and to better understand the functioning of the zinc half-electrode based on porous electrodes. The electrochemical cell described, compatible with X-ray experiments, is expected to be useful to the researchers in the field of electrochemistry.

Acknowledgements

Synchrotron radiation experiments were performed at the BL01B1 beamline of SPring-8 with the approval of the Japan Synchrotron Radiation Research Institute (project numbers of 2015B1398 and 2016A1297). We thank Dr T. Ina for his technical support during XAFS measurements at SPring-8.

Funding information

This work was supported by JSPS Grants-in-Aid for Scientific Researches (B) (No. 15H03877 to KF), and (A) (16H02411, to KM), and by the Core Research for Evolutional Science and Technology (CREST) program of JST (TA).

References

- Kim, H., Jeong, G., Kim, Y., Kim, J., Park, C. & Sohn, H. (2013). *Chem. Soc. Rev.* **42**, 9011–9034.
- Kinoshita, M. (2000). *Chem. Phys. Lett.* **326**, 551–557.
- Kinoshita, M. (2004). *J. Solution Chem.* **33**, 661–687.
- Koda, R., Fukami, K., Sakka, T. & Ogata, Y. H. (2013). *ECS Electrochem. Lett.* **2**, D9–D11.
- Koyama, A., Fukami, K., Suzuki, Y., Kitada, A., Sakka, T., Abe, T., Murase, K. & Kinoshita, M. (2016). *J. Phys. Chem. C*, **120**, 24112–24120.
- Li, Y. & Dai, H. (2014). *Chem. Soc. Rev.* **43**, 5257–5275.
- Li, Z., Huang, J., Liaw, B. Y., Metzler, V. & Zhang, J. (2014). *J. Power Sources*, **254**, 168–182.
- Muñoz-Noval, A., Fukami, K., Koyama, A., Kuruma, T., Kitada, A., Murase, K., Abe, T., Sakka, T. & Hayakawa, S. (2017). *J. Phys. Chem. C*, **121**, 18047–18056.
- Ravel, B. & Newville, M. (2005). *J. Synchrotron Rad.* **12**, 537–541.
- Xu, W., Wang, J., Ding, F., Chen, L., Nasybulin, E., Zhang, Y. & Zhang, J. (2014). *Energy Environ. Sci.* **7**, 513–537.